Lifetime measurements in ^{138}Nd

F. L. Bello Garrote,[1] A. Görgen,[1] C. Mihai,[2] T. Abraham,[3] L. Crespo Campo,[1] J.-P. Delaroche,[4] D. Filipescu,[2,5] N. M. Florea,[2] I. Gheorghe,[2] D. G. Ghita,[2] M. Girod,[4] T. Glodariu,[2,*] K. Hadyńska-Klęk,[1] M. Klintefjord,[1] J. Libert,[4] R. Lica,[2] T. Marchlewski,[3] N. Marginean,[2] R. Marginean,[2] I. Mitu,[2,5] A. Negret,[2] C. R. Nita,[2] F. Nowacki,[6] A. Olacel,[2] S. Pascu,[2] T. Renstrøm,[1] E. Sahin,[1] S. Siem,[1] J. Srebrny,[3] A. Stolarz,[3] L. Stroe,[2] S. Toma,[2,7] T. G. Tornyi,[1,8] and A. Tucholski[3]

[1]*Department of Physics, University of Oslo, NO-0316 Oslo, Norway*
[2]*Horia Hulubei National Institute of Physics and Nuclear Engineering, RO-077125 Bucharest, Romania*
[3]*Heavy Ion Laboratory, University of Warsaw, PL-02-093 Warsaw, Poland*
[4]*CEA, DAM, DIF, FR-91297 Arpajon Cedex, France*
[5]*Extreme Light Infrastructure Nuclear Physics, RO-077125 Bucharest, Romania*
[6]*Institute Pluridisciplinaire Hubert Curien, 23 Rue du Loess, FR-67037 Strasbourg Cedex 2, France*
[7]*Department of Physics, Politehnica University of Bucharest, RO-060042, Bucharest, Romania*
[8]*Institute of Nuclear Research of the Hungarian Academy of Sciences (MTA ATOMKI), HU-4001 Debrecen, Hungary*

(Received 21 April 2018; published 13 June 2018)

Lifetimes of several short-lived excited states in ^{138}Nd were measured with the ROSPHERE array at IFIN-HH, Bucharest, using the recoil-distance Doppler shift technique following the ^{123}Sb(^{19}F,4n) reaction. The resulting electromagnetic transition probabilities are compared to large-scale shell model calculations and to constrained Hartree-Fock-Bogoliubov calculations with the Gogny D1S interaction, configuration mixing, and a five-dimensional collective Hamiltonian formalism. The onset of collectivity in Nd isotopes below the $N = 82$ shell closure and the deformation induced by the alignment of protons and neutron holes in the $h_{11/2}$ orbitals are discussed.

DOI: 10.1103/PhysRevC.97.064310

I. INTRODUCTION

Nuclei with atomic number $Z \approx 60$ and neutron number $N \approx 78$ are thought to be soft with respect to the triaxial degree of deformation. Calculations based on modified harmonic oscillator [1] or Woods-Saxon [2] potentials, and self-consistent Hartree-Fock-Bogoliubov (HFB) calculations using Skyrme [3] or Gogny [4] interactions, predicted triaxial ground-state shapes for the nuclei in this region. Systematic studies of axial shape asymmetries for the ground state within the finite-range liquid drop model identified this region as one of two in the nuclear chart where deviations from axial symmetry are most pronounced (the other being near ^{108}Ru) [5].

At intermediate spins, the structure of nuclei in this region is strongly influenced by proton excitations at the bottom and neutron-hole excitations at the top of the $h_{11/2}$ shell. Several 10^+ isomeric states associated with the $\pi h_{11/2}^2$ or $\nu h_{11/2}^{-2}$ configuration, at very similar excitation energies, are found in the region [6]. The alignment of $h_{11/2}$ protons is understood to drive a γ-soft core towards prolate shape, whereas the alignment of $h_{11/2}$ neutron holes induces oblate shape. The proton or neutron character of some of these states has been confirmed by g-factor measurements [7]. In ^{138}Nd the 10^+ isomeric state at 3175 keV [8,9] was found to have a neutron character [10], whereas the 10^+ state at 3701 keV, which is not isomeric, has been associated with the $\pi h_{11/2}^2$ configuration, and lies at higher excitation energy due to the lower Fermi surface with respect to the $\pi h_{11/2}$ orbital [11].

The quasirotational bands on top of the 10^+ states with proton and neutron configurations, in ^{138}Nd [11,12], as well as in ^{140}Sm and ^{142}Gd [13,14], were found to be very similar to the ground-state bands in the respective $(Z-2)$ and $(N+2)$ cores. Lifetime measurements above the 10^+ states in ^{140}Sm support the notion of shape coexistence at intermediate spins [15]. Electromagnetic matrix elements obtained from Coulomb excitation [16] and lifetime measurements [17] for ^{140}Sm and their comparison to theoretical calculations suggest weak deformation and softness to γ deformation with an equilibrium shape of $\gamma \approx 30^\circ$ near the ground state. For ^{138}Nd, indication of γ softness comes from the low excitation energy of the γ-vibrational band [18] and the observation of a two-phonon γ band [19]. Studies of ^{138}Nd at high angular momentum revealed rotational bands that can be associated with strongly deformed axially symmetric [20] and triaxial shapes [21–23].

To obtain a more quantitative understanding of the shape evolution of Nd nuclei from spherical shape at the $N = 82$ shell closure to relatively large deformation for the most neutron-deficient isotopes [24], possible shape coexistence at intermediate spins, and the role of triaxiality and γ softness near the ground state, measurements of electromagnetic transition strengths are needed. Except for the isomeric 10^+ state at 3175 keV [8,9] and the 7^- state at 2321 keV (for which only an estimated value of the lifetime has been given [25]), the lifetimes of excited states in ^{138}Nd are completely unknown. In this work we report on lifetime measurements using the

[*]Deceased.

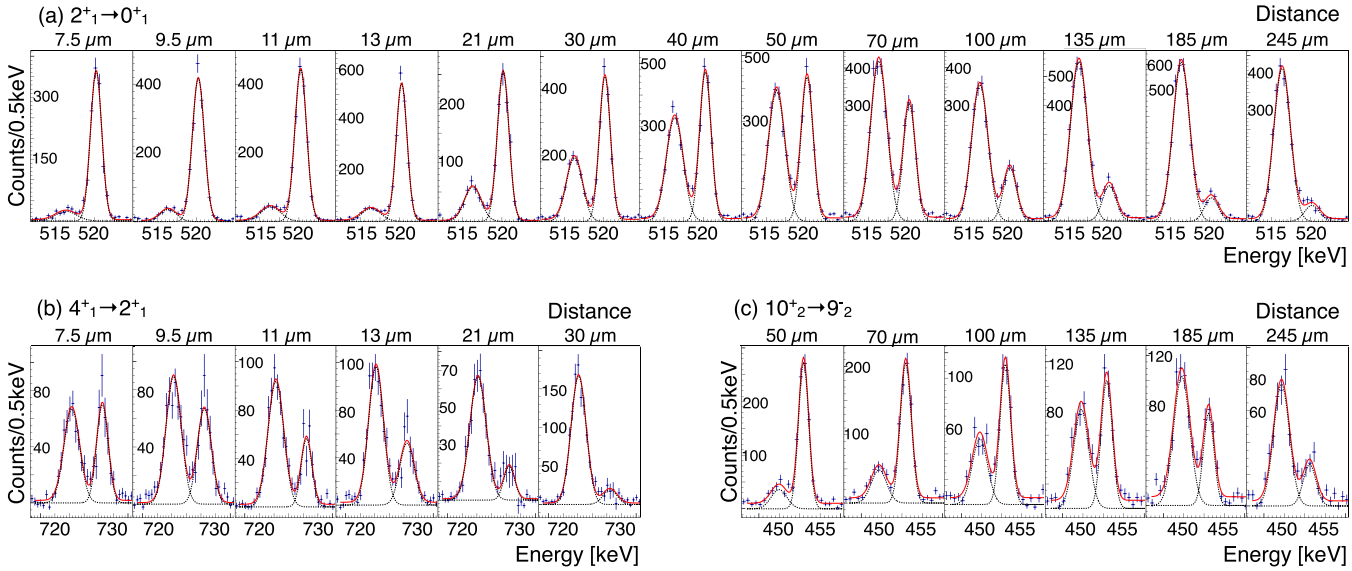

FIG. 1. Background-subtracted spectra showing the Doppler-shifted and unshifted components of the $2^+_1 \rightarrow 0^+_1$ (a), $4^+_1 \rightarrow 2^+_1$ (b), and $10^+_2 \rightarrow 9^-_2$ (c) transitions, measured with the backward detectors for different distances. The transitions were detected in coincidence with the shifted components of γ rays feeding the 2^+_1, 4^+_1, and 10^+_2 states, respectively (see Table I).

recoil-distance Doppler shift (RDDS) method for various states in ^{138}Nd.

II. EXPERIMENTAL SETUP

The present lifetime measurement was performed using the ^{123}Sb(^{19}F,4n)^{138}Nd reaction at the 9 MV Tandem Accelerator facility at the IFIN-HH in Bucharest-Magurele. The target, which was made at the Target Preparation Laboratory of the IFIN-HH [26], consisted of a 0.5 mg/cm^2 thick layer of ^{123}Sb that was deposited on a 5 mg/cm^2 thick gold backing to facilitate the stretching of the foil. The ^{19}F beam of 80 MeV was first passing through the gold backing before reacting with the ^{123}Sb layer at an energy of approximately 68 MeV. At this relatively low energy the 4n reaction leading to ^{138}Nd is the dominant reaction channel. γ rays following Coulomb excitation of the gold backing were strongly suppressed by requiring the detection of γ-γ coincidences. Nuclei recoiling from the target were stopped in another gold foil of 5 mg/cm^2 thickness. The distance between the target and the stopper foils was adjusted using the Köln-Bucharest Plunger device [27], and the γ rays were measured with the ROSPHERE array [27]. Thirteen different target-to-stopper distances ranging from 7.5 to 245 μm were set during the experiment, with an average measuring time of 18 h per distance and an average beam intensity of ∼3 pnA.

III. DATA ANALYSIS AND EXPERIMENTAL RESULTS

The decay path of the excited states in ^{138}Nd is rather fragmented (see the level scheme of Fig. 3), and a large portion of the γ-ray intensity passes through either the 5^-_1 or the 7^-_1 state at 1990 and 2321 keV, respectively, both of which have a relatively long lifetime. To avoid the problem of possible unobserved feeding and unknown lifetimes of feeding levels, the lifetimes of the states of interest were measured using the differential decay curve method (DDCM) [28–30], gating on the Doppler-shifted components of a transition that directly feeds the state of interest. Ten Compton-suppressed large volume HPGe detectors of the ROSPHERE array [27] were used in the analysis, five of them at 37° (forward) and the remaining five at 143° (backward) with respect to the beam direction. The Doppler-shifted and unshifted components of the transitions of interest can be clearly resolved for these angles. The average velocity of the recoiling nuclei was obtained from the energy difference between the shifted and unshifted components of the $2^+_1 \rightarrow 0^+_1$, $4^+_1 \rightarrow 2^+_1$, and $6^+_1 \rightarrow 4^+_1$ transitions, measured for several distances and for both backward and forward detectors. The resulting average velocity was found to be $v = 2.81(1)$ μm/ps [$v/c = 0.94(1)$]%.

The γ-γ coincidence events were sorted into three matrices according to the angles of the detectors in which the γ rays were detected: forward-forward, forward-backward, and backward-backward. The DDCM analysis was performed independently for the forward and backward angles, and the final lifetime values were obtained from the weighted average of the forward and backward measurements. Background-subtracted spectra showing the Doppler-shifted and unshifted components of the $2^+_1 \rightarrow 0^+_1$, $4^+_1 \rightarrow 2^+_1$, and $10^+_2 \rightarrow 9^-_2$ transitions measured for different distances are presented in Fig. 1 to illustrate the quality of the data. The transitions shown in Fig. 1 were detected in the backward detectors in coincidence with the shifted components of the 729, 884, and 503 keV γ rays that respectively feed the 2^+_1, 4^+_1, and 10^+_2 states.

Figure 2 shows the normalized values of the intensities of the shifted and unshifted components of the $2^+_1 \rightarrow 0^+_1$ transition, measured for different distances using the backward detectors. The intensities of the transitions were normalized to the total number of counts in the total projections of the corresponding γ-γ matrices to account for the duration of the

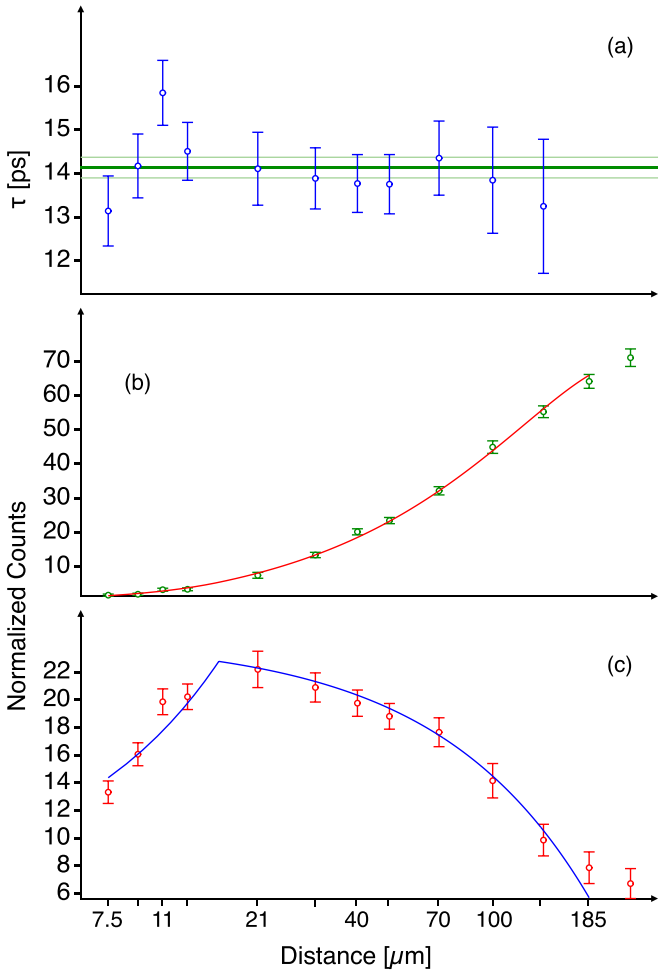

FIG. 2. Normalized values of the intensities of the shifted (b) and unshifted (c) components of the $2_1^+ \rightarrow 0_1^+$ transition, measured for different distances using the backward detectors. The lifetimes obtained for the different distances are shown in (a), where the horizontal lines indicate the weighted average and its uncertainty.

measurements at each distance and any changes in the beam intensity. Following the DDCM [30] procedure, the decay curves in Fig. 2 were fitted simultaneously using piece-wise continuous polynomials. A lifetime value was obtained for each distance inside the region of sensitive distances using the intensity of the unshifted component, the derivative of the intensity curve for the shifted component, and the recoil velocity. The lifetimes obtained for individual distances were finally combined in a weighted average. The uncertainties of the lifetimes were dominated by the statistical uncertainties arising from the fit of the shifted and unshifted peaks.

The same technique was used to determine the lifetimes of all states for which the shifted and unshifted components of their decay transitions showed sufficient variation. The results are shown in Table I and Fig. 3. In the case of the 5_1^- state, the intensity of the shifted component showed a relative increase only at the three largest distances. Because of the large uncertainties in the calculation of the derivatives, it was not possible to extract a reliable value of the lifetime, and only a minimum value is reported.

TABLE I. Lifetimes measured in the present work. The energies of the fitted transitions are indicated (E_γ), as well as the transitions used for gating. The lifetimes are the averages of the results obtained from the backward and forward detectors.

E_x[keV]	J_n^π	E_γ[keV]	Gate	τ[ps]
521	2_1^+	521	$4_1^+ \rightarrow 2_1^+$	13.9(2)
1014	2_2^+	493	$3_1^+ \rightarrow 2_2^+$	8.7(7)
1250	4_1^+	729	$6_1^+ \rightarrow 4_1^+$	1.9(2)
1990	5_1^-	740	$7_1^- \rightarrow 5_1^-$	>57
2691	7_2^-	470	$9_2^- \rightarrow 7_2^-$	9.5(8)
3701	10_2^+	454	$12_2^+ \rightarrow 10_2^+$	47.8(11)
3821	12_1^+	647	$14_2^+ \rightarrow 12_1^+$	9.6(6)
4203	12_2^+	503	$14_1^+ \rightarrow 12_2^+$	14.0(4)

IV. DISCUSSION

The $B(E1)$ and $B(E2)$ values resulting from the measured lifetimes are summarized in Table II. To obtain these values it was assumed that the transitions have pure $E1$ or $E2$ multipolarity, respectively, except for the case of the $7_2^- \rightarrow 7_1^-$ transition, which can be of mixed $M1/E2$ character. As the mixing ratio for this transition is not known, no reduced transition probability was deduced from the lifetime of the 7_2^- state. In those cases where the decay of a state is fragmented to multiple final states, previously published branching ratios [18,19,31] were used to determine the transition strengths.

The $B(E2; 2_1^+ \rightarrow 0_1^+)$ value for ^{138}Nd corresponds to 36(1) Weisskopf units (W.u.). This transition strength is similar to

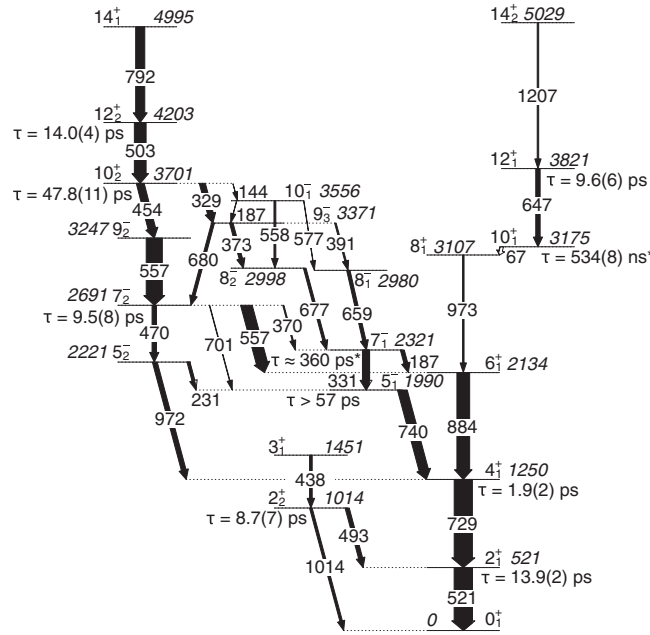

FIG. 3. Partial level scheme of ^{138}Nd, based on Ref. [31]. The lifetimes of the states measured in the present work are shown together with the previously known lifetimes of the 10_1^+ state [8,9] and the 7_1^- state [25], which are marked with an asterisk (⋆). The widths of the arrows indicate the relative intensities of the transitions.

TABLE II. Reduced transition probabilities for $E1$ and $E2$ transitions in ^{138}Nd. The branching ratios are those in Ref. [31], with the exception of the 2_2^+ state, for which the averages of the values reported in Refs. [18,19] are used. The lifetimes of the states used for the calculation of the $B(E1)$ and $B(E2)$ values are those in Table I and Fig. 3, and the internal conversion coefficients were obtained from Ref. [32].

I_i	I_f	E_γ [keV]	$E\lambda$	branch [%]	$B(E\lambda; I_i \to I_f)$ [e^2fm$^{2\lambda}$]
2_1^+	0_1^+	521	$E2$	100	1520(30)
2_2^+	0_1^+	1014	$E2$	31(6)	27(6)
2_2^+	2_1^+	493	$E2$	69(6)	2190(260)
4_1^+	2_1^+	729	$E2$	100	2070(270)
5_1^-	4_1^+	740	$E1$	100	$<2.7\times10^{-5}$
7_1^-	5_1^-	331	$E2$	92(1)	$\approx$500
7_1^-	6_1^+	187	$E1$	8(2)	$\approx2\times10^{-5}$
7_2^-	5_1^-	701	$E2$	2.7(6)	14(3)
7_2^-	6_1^+	557	$E1$	66(6)	$2.5(4)\times10^{-4}$
7_2^-	5_2^-	470	$E2$	24(3)	890(280)
7_2^-	7_1^-	370	$M1/E2$	7(1)	
10_1^+	8_1^+	67	$E2$	100	107(8)
10_2^+	9_2^-	454	$E1$	56(6)	$7.8(10)\times10^{-5}$
10_2^+	9_3^-	329	$E1$	43(4)	$1.6(3)\times10^{-4}$
10_2^+	10_1^-	144	$E1$	1.0(4)	$4(2)\times10^{-5}$
12_1^+	10_1^+	647	$E2$	100	750(60)
12_2^+	10_2^+	503	$E2$	100	1790(80)

the value of 39(4) W.u. that was measured in the isotone ^{136}Ce [33], but smaller than 49(4) W.u. in ^{140}Sm [17]. This finding is consistent with the expectation that collectivity increases with the number of valence protons. The relatively strong increase of the $B(E2; 2_1^+ \to 0_1^+)$ value from ^{138}Nd to ^{140}Sm seems, on the other hand, surprising because the excitation energies for the 2_1^+ and 4_1^+ states are very similar for both nuclei.

The evolution of transition strengths in the ground-state bands of even-even Nd isotopes below the $N = 82$ shell closure is shown in Fig. 4, where the available experimental data are compared to microscopic calculations based on constrained Hartree-Fock-Bogoliubov theory using the Gogny D1S interaction [34,35] and mapping to the five-dimensional collective Hamiltonian (5DCH) for quadrupole excitations. The method used in the calculations is described in more detail elsewhere [36]. The calculations predict a smooth onset of collectivity with decreasing neutron number and generally reproduce the trend of the experimental values for the $2_1^+ \to 0_1^+$ and $4_1^+ \to 2_1^+$ transitions. Data for the $6_1^+ \to 4_1^+$ transitions is too sparse to draw any conclusions. For the case of ^{138}Nd the calculations reproduce the $B(E2; 2_1^+ \to 0_1^+)$ value well, but find a somewhat too large $B(E2; 4_1^+ \to 2_1^+)$ value. The 5DCH calculations also reproduce the strong increase in $B(E2; 2_1^+ \to 0_1^+)$ value from ^{138}Nd to ^{140}Sm and find 41 and 48 W.u., respectively.

The low-lying states in ^{138}Nd show typical features of a transitional nucleus, for example, an energy ratio of $E(4_1^+)/E(2_1^+) = 2.40$. The ratio of $B(E2)$ values is $B(E2; 4_1^+ \to 2_1^+)/B(E2; 2_1^+ \to 0_1^+) = 1.36(15)$, similar to

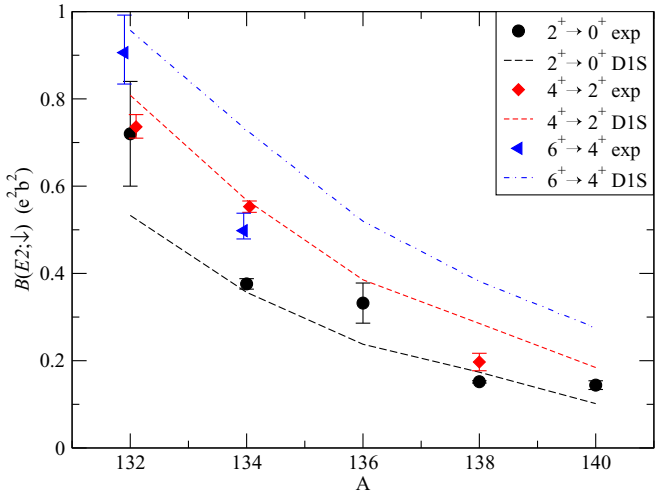

FIG. 4. Experimental $B(E2;\downarrow)$ values for transitions in the ground-state band of ^{132}Nd [37,38], ^{134}Nd [39], ^{136}Nd [40], ^{138}Nd (present work), and ^{140}Nd [41] compared to theoretical calculations based on the 5DCH approach with the Gogny D1S interaction.

what is found in ^{140}Sm, where $E(4_1^+)/E(2_1^+) = 2.35$ and $B(E2; 4_1^+ \to 2_1^+)/B(E2; 2_1^+ \to 0_1^+) = 1.30(14)$ [16]. A comparison of the experimental excitation energies and $B(E2)$ transition probabilities with theoretical calculations using the 5DCH approach and with shell model calculations for selected states is presented in Table III. The Gogny calculations reproduce the energy ratios for the states in the ground-state band, but the absolute energies are overestimated by about 20%. Such an overestimation of energies of the Gogny calculations has been observed already earlier for transitional, γ-soft nuclei [16]. It should be noted that the 5DCH approach contains no free parameters other that those specifying the Gogny D1S interaction, which is used globally for all nuclei.

TABLE III. Experimental excitation energies (in keV) of selected states in ^{138}Nd and reduced transition probabilities $B(E2; I_i \to I_f)$ (in e^2fm^4) between them compared to theoretical calculations using a 5DCH Hamiltonian and the Gogny D1S interaction and to large-scale shell model calculations (see text for details).

	Exp.	5DCH	SM
$E(2_1^+)$	521	660	513
$E(2_2^+)$	1014	1461	
$E(4_1^+)$	1250	1541	1346
$E(6_1^+)$	2134	2610	2345
$E(8_1^+)$	3107		3274
$E(10_1^+)$	3175		3247
$E(10_2^+)$	3701		4214
$E(12_1^+)$	3821		3842
$B(E2; 2_1^+ \to 0_1^+)$	1520(30)	1736	1945
$B(E2; 2_2^+ \to 0_1^+)$	27(6)	15	
$B(E2; 2_2^+ \to 2_1^+)$	2190(260)	2531	
$B(E2; 4_2^+ \to 2_1^+)$	2070(270)	2853	2803
$B(E2; 10_1^+ \to 8_1^+)$	107(8)		634
$B(E2; 12_1^+ \to 10_1^+)$	750(60)		885

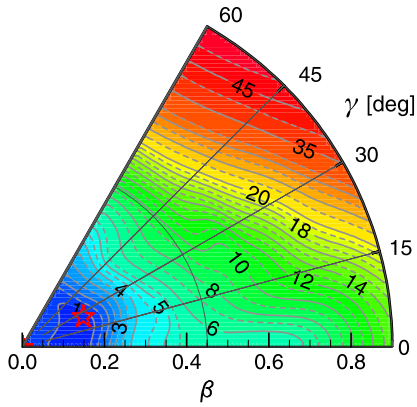

FIG. 5. Potential energy surface (PES) for the ground-state of ^{138}Nd based on constrained Hartree-Fock-Bogoliubov calculations with the Gogny D1S interaction. The lines and numbers indicate the potential energy in MeV.

Evidence for triaxiality was found in neighboring ^{140}Sm [16]. The potential energy surface (Fig. 5) for ^{138}Nd calculated with the Gogny D1S interaction is shown in Fig. 5. Similar to ^{140}Sm, the PES for ^{138}Nd features a rather shallow spherical minimum that is flat in both β and γ direction. The mean dynamic deformation in the PES is found at $\langle\beta\rangle = 0.17$ and $\langle\gamma\rangle = 27^\circ$, indicated by star in Fig. 5. The predicted γ softness is consistent with the observation of a very low-lying quasi-γ band with the excitation energy of the 2_2^+ state below that of the 4_1^+ state [18]. The energy ratio $E(2_2^+)/E(2_1^+) = 1.95$ is close to what is expected for a nucleus with maximum triaxiality. The $B(E2; 2_2^+ \rightarrow 2_1^+)$ and $B(E2; 2_2^+ \rightarrow 0_1^+)$ values are well reproduced by the Gogny calculations (c.f. Table III), and are consistent with the interpretation of pronounced triaxiality near the ground state of ^{138}Nd, with the decay from the 2_2^+ state to the 2_1^+ state strongly favored over that to the ground state. The calculated spectroscopic quadrupole moments for the 2_1^+ and 2_2^+ states are $Q_s(2_1^+) = -30\ e\text{fm}^2$ and $Q_s(2_2^+) = +31\ e\text{fm}^2$, respectively.

To gain further insight into the structure of the low-lying states in ^{138}Nd, large-scale shell model calculations were carried out using a ^{100}Sn core with a valence space including the $g_{7/2}$, $d_{3/2}$, $s_{1/2}$, $d_{5/2}$, and $h_{11/2}$ orbitals for both protons and neutrons, and the effective GCN5082 interaction [42], based on a realistic renormalized G matrix with phenomenological monopole constraints. Similar to previous shell model calculations for ^{140}Sm [16], a seniority truncation scheme was introduced to limit the otherwise prohibitively large basis dimensions. Effective charges of $\epsilon_\pi = 1.65$ for protons and $\epsilon_\nu = 0.65$ for neutrons were used to determine the transition probabilities. Results from the shell model calculations are presented in Table III and compared to experimental excitation energies and transition strengths and results from the 5DCH calculations based on the Gogny D1S interaction. While the 5DCH calculations were limited to states with $I^\pi \leqslant 6^+$, the shell model calculations were extended up to spin 12^+.

The energies of the yrast states with even spin and positive parity calculated in the shell model are in relatively good agreement with the experimental values. In the calculation, the order of the 8_1^+ and 10_1^+ states is inverted with the 10_1^+ state lying just below the 8_1^+ state, but the absolute energies are well reproduced. The $B(E2)$ values from the shell model calculations for the low-lying states are somewhat too large. The same effective charges were used as in the calculations for ^{140}Sm [16], where a better agreement was achieved. A possible explanation could be that the calculations for ^{140}Sm, which have even larger dimension, were not fully converged and that somewhat smaller effective charges might be more appropriate for this mass region.

The excitation energy of the isomeric 10_1^+ state is well reproduced. However, the calculated $B(E2; 10_1^+ \rightarrow 8_1^+)$ value is too large. The 10_1^+ isomer is understood as having an aligned $\nu h_{11/2}^{-2}$ configuration [11,12]. It is again conceivable that the calculations are not fully converged and that the wave function of the 10_1^+ state is therefore more mixed, resulting in a larger transition strength. The $B(E2; 12_1^+ \rightarrow 10_1^+)$ transition strength, on the other hand, is well reproduced. The calculated energy of the 10_2^+ state is too high, probably because of the too constricted truncation scheme. With an incomplete level scheme and a too restricted model space for the states with higher spin, the shell model calculations cannot contribute more to the understanding of experimental transition probabilities. Instead, it is interesting to discuss the measured $B(E2)$ values within the systematics of the neighboring nuclides.

The similarity between the quasirotational band built on the $\pi(h_{11/2}^2)_{10^+}$ state in ^{138}Nd, the $\pi h_{11/2}$ band in ^{137}Pr, and the ground-state band in ^{136}Ce on the one hand, and between the $\nu(h_{11/2}^{-2})_{10^+}$ band in ^{138}Nd, the $\nu h_{11/2}^{-1}$ band in ^{139}Nd, and the ground-state band in ^{140}Nd on the other hand, was already pointed out and discussed by de Angelis *et al.* [11]. Corresponding systematics were discussed for the bands built on the 10^+ isomers associated with the $\pi h_{11/2}^2$ and $\nu h_{11/2}^{-2}$ configurations in ^{140}Sm and ^{142}Gd by Starzecki *et al.* [13]. The newly measured $B(E2)$ values complete the systematics and allow a comparison also for the transition probabilities between the respective states, as shown in Fig. 6.

It has been discussed earlier that the alignment of $h_{11/2}$ protons induces prolate shape, whereas the alignment of $h_{11/2}$ neutron holes induces oblate shapes [11]. The energy spacings in the bands built on the $\pi(h_{11/2}^2)_{10^+}$ configuration in ^{138}Nd, ^{140}Sm, and ^{142}Gd suggest a higher collectivity compared to the bands built on the $\nu(h_{11/2}^{-2})_{10^+}$ configuration. As can be seen in Fig. 6, the $B(E2)$ values for the bands built on the $h_{11/2}$ proton configuration are indeed higher than for the bands built on the aligned $h_{11/2}$ neutron holes. Consistent with the similarity of the transition energies, also the $B(E2)$ values of the $\pi(h_{11/2}^2)_{10^+}$ bands show a remarkable similarity with the ground-state bands in the $Z-2$ core nuclei. The $B(E2)$ values in the $\nu(h_{11/2}^{-2})_{10^+}$ bands are slightly smaller than those in the ground-state bands of the $N+2$ cores, but the overall systematic picture is very consistent.

V. SUMMARY AND CONCLUSIONS

Lifetimes have been measured for several excited states in ^{138}Nd using the recoil-distance Doppler shift technique following the ^{123}Sb(^{19}F,4n) fusion-evaporation reaction and

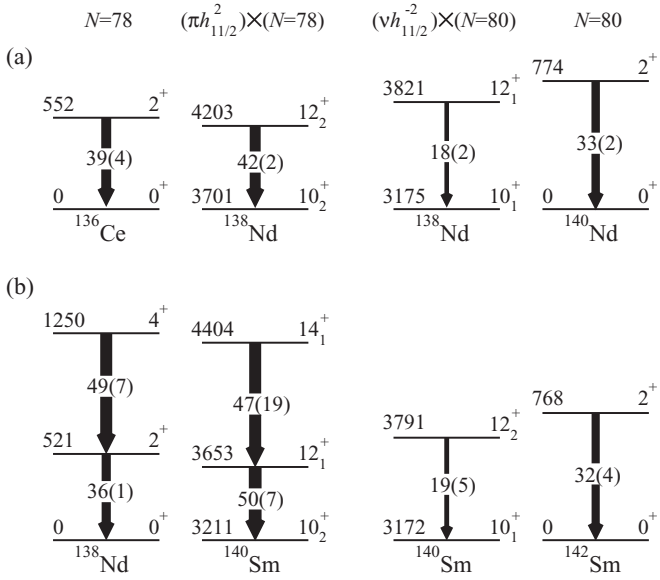

FIG. 6. Comparison of $B(E2)$ values for transitions in the quasirotational bands on top of the 10^+_1 and 10^+_2 states in ^{138}Nd (a) and ^{140}Sm (b) with $B(E2)$ values of transitions in the ground-state bands of the respective $(Z-2)$ and $(N+2)$ cores. The $B(E2)$ values for ^{136}Ce [33], ^{138}Nd (present work), ^{140}Nd [41], ^{140}Sm [15], and ^{142}Sm [43] are given in Weisskopf units, and the widths of the transitions are proportional to the corresponding $B(E2)$ values.

the ROSPHERE germanium detector array. The measured lifetimes yield $B(E2)$ transition probabilities for transitions within the ground-state band, the quasi-γ band, and the bands built on top of the $\nu(h^{-2}_{11/2})_{10^+}$ and $\pi(h^{2}_{11/2})_{10^+}$ states. In addition, several $B(E1)$ and $B(E2)$ transition probabilities involving negative-parity states were measured.

The results were compared to large-scale shell model calculations using a ^{100}Sn core and the GCN5082 interaction, and to beyond-mean-field calculations based on constrained Hartree-Fock-Bogoliubov calculations using the Gogny D1S interaction and mapping to a five-dimensional collective Hamiltonian. The results suggest that the states near the ground state have small deformation with pronounced triaxiality and softness in both the β and γ degrees of freedom.

The measured $B(E2)$ values above the 10^+ states support the picture of shape coexistence between prolate and oblate shapes with $h^2_{11/2}$ proton and $h^{-2}_{11/2}$ neutron configurations, respectively: the alignment of two $h_{11/2}$ protons results in a quasirotational band that is very similar to the ground-state band in the ^{136}Ce core; similarly, the states above the aligned neutron configuration have properties that are similar to the ground-state band in the ^{140}Nd core. The same analogy is found for the band built on the $\pi h^2_{11/2}$ configuration in ^{140}Sm and the ground-state band in ^{138}Nd. Beyond-mean field calculations up to higher spins and larger shell-model calculations with less truncation would be needed to draw further conclusions. Calculations for the transition probabilities involving negative-parity states are currently beyond the reach of the theoretical models.

ACKNOWLEDGMENTS

This work was supported by The Research Council of Norway under project Grants No. 213442 and No. 205528, and the Romanian Research and Innovation Ministry under contracts no. PN 18090102 and 03-CERN. The authors would like to thank the technical staff at the IFIN-HH Tandem Laboratory for their support during the experiment.

[1] I. Ragnarsson *et al.*, Nucl. Phys. A **233**, 329 (1974).
[2] B. D. Kern *et al.*, Phys. Rev. C **36**, 1514 (1987).
[3] N. Redon *et al.*, Phys. Lett. B **181**, 223 (1986).
[4] M. Girod and B. Grammaticos, Phys. Rev. C **27**, 2317 (1983).
[5] P. Möller, R. Bengtsson, B. G. Carlsson, P. Olivius, and T. Ichikawa, Phys. Rev. Lett. **97**, 162502 (2006).
[6] The Evaluated Nuclear Structure Data File, ENSDF, http://www.nndc.bnl.gov/ensdf/.
[7] N. J. Stone, INDC(NDS)-0658 (2014).
[8] A. Vancraeyenest, C. M. Petrache, D. Guinet, P. T. Greenlees, U. Jakobsson, R. Julin, S. Juutinen, S. Ketelhut, M. Leino, M. Nyman, P. Peura, P. Rahkila, P. Ruotsalainen, J. Saren, C. Scholey, J. Sorri, J. Uusitalo, P. Jones, C. Ducoin, P. Lautesse, C. Mancuso, N. Redon, O. Stezowski, P. Desesquelles, R. Leguillon, A. Korichi, T. Zerrouki, D. Curien, and A. Takashima, Phys. Rev. C **87**, 064303 (2013).
[9] N. Yoshikawa, Nucl. Phys. A **243**, 143 (1975).
[10] D. Riegel, Phys. Rev. Lett. **48**, 516 (1982).
[11] G. de Angelis, M. A. Cardona, M. De Poli, S. Lunardi, D. Bazzacco, F. Brandolini, D. Vretenar, G. Bonsignori, M. Savoia, R. Wyss, F. Terrasi, and V. Roca, Phys. Rev. C **49**, 2990 (1994).
[12] M. Müller-Veggian *et al.*, Nucl. Phys. A **344**, 89 (1980).
[13] W. Starzecki *et al.*, Phys. Lett. B **200**, 419 (1988).
[14] S. Lunardi, D. Bazzacco, G. Nardelli, F. Soramel, J. Rico, E. Maglione, M. De Poli, and G. de Angelis, Phys. Rev. C **42**, 174 (1990).
[15] M. A. Cardona, S. Lunardi, D. Bazzacco, G. de Angelis, and V. Roca, Phys. Rev. C **44**, 891 (1991).
[16] M. Klintefjord, K. Hadynska-Klek, A. Gorgen, C. Bauer, F. L. BelloGarrote, S. Bonig, B. Bounthong, A. Damyanova, J. P. Delaroche, V. Fedosseev, D. A. Fink, F. Giacoppo, M. Girod, P. Hoff, N. Imai, W. Korten, A. C. Larsen, J. Libert, R. Lutter, B. A. Marsh, P. L. Molkanov, H. Naidja, P. Napiorkowski, F. Nowacki, J. Pakarinen, E. Rapisarda, P. Reiter, T. Renstrom, S. Rothe, M. D. Seliverstov, B. Siebeck, S. Siem, J. Srebrny, T. Stora, P. Thole, T. G. Tornyi, G. M. Tveten, P. VanDuppen, M. J. Vermeulen, D. Voulot, N. Warr, F. Wenander, H. DeWitte, and M. Zielinska, Phys. Rev. C **93**, 054303 (2016).
[17] F. L. B. Garrote *et al.*, Phys. Rev. C **92**, 024317 (2015).
[18] J. Deslauriers, S. C. Gujrathi, and S. K. Mark, Z. Phys. A **303**, 151 (1981).
[19] H. J. Li, Z. G. Xiao, S. J. Zhu, E. Y. Yeoh, Y. X. Liu, Y. Sun, Z. Zhang, R. S. Wang, H. Yi, W. H. Yan, Q. Xu, X. G. Wu, C. Y. He, Y. Zheng, G. S. Li, C. B. Li, H. W. Li, J. J. Liu, S. P. Hu, J. L. Wang, and S. H. Yao, Phys. Rev. C **87**, 057303 (2013).

[20] S. Lunardi, D. Bazzacco, C. A. Ur, M. Axiotis, G. de Angelis, E. Farnea, T. Kröll, S. M. Lenzi, G. Lo Bianco, N. Mărginean, T. Martinez, R. Menegazzo, D. R. Napoli, P. Pavan, C. M. Petrache, B. Quintana, C. Rossi Alvarez, A. Saltarelli, R. Venturelli, and I. Ragnarsson, Phys. Rev. C **69**, 054302 (2004).
[21] C. M. Petrache, G. Lo Bianco, D. Ward, A. Galindo-Uribarri, P. Spolaore, D. Bazzacco, T. Kröll, S. Lunardi, R. Menegazzo, C. Rossi Alvarez, A. O. Macchiavelli, M. Cromaz, P. Fallon, G. J. Lane, W. Gast, R. M. Lieder, G. Falconi, A. V. Afanasjev, and I. Ragnarsson, Phys. Rev. C **61**, 011305(R) (1999).
[22] C. M. Petrache, S. Frauendorf, M. Matsuzaki, R. Leguillon, T. Zerrouki, S. Lunardi, D. Bazzacco, C. A. Ur, E. Farnea, C. Rossi Alvarez, R. Venturelli, and G. de Angelis, Phys. Rev. C **86**, 044321 (2012).
[23] C. M. Petrache, I. Ragnarsson, H.-L. Ma, R. Leguillon, T. Zerrouki, D. Bazzacco, and S. Lunardi, Phys. Rev. C **91**, 024302 (2015).
[24] R. Moscrop *et al.*, Nucl. Phys. A **499**, 565 (1989).
[25] S. C. Pancholi and M. J. Martin, Nucl. Data Sheets B **18**, 167 (1976); J. van Klinken *et al.*, KFK-1768 (1973).
[26] N. M. Florea *et al.*, J. Radioanal. Nucl. Chem. **305**, 707 (2015).
[27] D. Bucurescu *et al.*, Nucl. Instrum. Methods Phys. Res. A **837**, 1 (2016).
[28] A. Dewald, S. Harissopulos, and P. von Brentano, Z. Phys. A **334**, 163 (1989).
[29] G. Böhm *et al.*, Nucl. Instrum. Methods Phys. Res. A **329**, 248 (1993).
[30] A. Dewald, O. Möller, and P. Petkov, Prog. Part. Nucl. Phys. **67**, 786 (2012).
[31] J. Chen, Nucl. Data Sheets **146**, 1 (2017).
[32] Conversion Coefficient Calculator, BrIcc, http://bricc.anu.edu.au.
[33] S. Raman, C. W. Nestor, Jr., and P. Tikkanen, At. Data Nucl. Data Tables **78**, 1 (2001); Yu. P. Gangrsky *et al.*, JINR-P15-89-157 (1989).
[34] J. Dechargé and D. Gogny, Phys. Rev. C **21**, 1568 (1980).
[35] J. Berger, M. Girod, and D. Gogny, Comput. Phys. Commun. **63**, 365 (1991).
[36] J.-P. Delaroche, M. Girod, J. Libert, H. Goutte, S. Hilaire, S. Péru, N. Pillet, and G. F. Bertsch, Phys. Rev. C **81**, 014303 (2010).
[37] B. Pritychenko *et al.*, At. Data Nucl. Data Tables **107**, 1 (2016).
[38] R. Krücken *et al.*, Nucl. Phys. A **589**, 475 (1995).
[39] T. Klemme, A. Fitzler, A. Dewald, S. Schell, S. Kasemann, R. Kühn, O. Stuch, H. Tiesler, K. O. Zell, P. von Brentano, D. Bazzacco, F. Brandolini, S. Lunardi, C. M. Petrache, C. Rossi Alvarez, G. De Angelis, P. Petkov, and R. Wyss, Phys. Rev. C **60**, 034301 (1999).
[40] T. R. Saito *et al.*, Phys. Lett. B **669**, 19 (2008).
[41] C. Bauer, G. Rainovski, N. Pietralla, D. Bianco, A. Blazhev, T. Bloch, S. Bonig, A. Damyanova, M. Danchev, K. A. Gladnishki, T. Kroll, J. Leske, N. LoIudice, T. Moller, K. Moschner, J. Pakarinen, P. Reiter, M. Scheck, M. Seidlitz, B. Siebeck, C. Stahl, R. Stegmann, T. Stora, C. Stoyanov, D. Tarpanov, M. J. Vermeulen, D. Voulot, N. Warr, F. Wenander, V. Werner, and H. DeWitte, Phys. Rev. C **88**, 021302(R) (2013).
[42] A. Gniady, E. Caurier, and F. Nowacki (unpublished).
[43] R. Stegmann, C. Bauer, G. Rainovski, N. Pietralla, C. Stahl, S. Bonig, S. Ilieva, A. Blazhev, A. Damyanova, M. Danchev, K. Gladnishki, J. Jolie, R. Lutter, J. Pakarinen, D. Radeck, E. Rapisarda, P. Reiter, M. Scheck, B. Siebeck, T. Stora, P. Thole, T. Thomas, M. Thurauf, M. J. Vermeulen, D. Voulot, N. Warr, F. Wenander, V. Werner, and H. DeWitte, Phys. Rev. C **91**, 054326 (2015).